Wetland-estuarine-shelf interactions in the Plum Island Sound and Merrimack River in the Massachusetts coast

Liuzhi Zhao,[1] Changsheng Chen,[1,4,6] Joe Vallino,[4] Charles Hopkinson,[5] Robert C. Beardsley,[2] Huichan Lin,[1] and Jim Lerczak[6]

Received 27 December 2009; revised 2 June 2010; accepted 17 June 2010; published 16 October 2010.

[1] Wetland-estuarine-shelf interaction processes in the Plum Island Sound and Merrimack River system in the Massachusetts coast are examined using the high-resolution unstructured grid, finite volume, primitive equations, coastal ocean model. The computational domain covers the estuarine and entire intertidal area with a horizontal resolution of 10–200 m. Driven by five tidal constituents forcing at the open boundary on the inner shelf of the eastern coast of the Gulf of Maine, the model has successfully simulated the 3-D flooding/drying process, temporal variability, and spatial distribution of salinity as well as the water exchange flux through the water passage between the Plum Island Sound and Merrimack River. The model predicts a complex recirculation loop around the Merrimack River, shelf, and Plum Island Sound. During the ebb tide, salt water in the Plum Island Sound is injected into the Merrimack River, while during flood tide, a significant amount of the freshwater in the Merrimack River is forced into Plum Island Sound. This water exchange varies with the magnitude of freshwater discharge and wind conditions, with a maximum contribution of ~30%–40% variability in salinity over tidal cycles in the mouth of the Merrimack River. Nonlinear tidal rectification results in a complex clockwise residual recirculation loop around the Merrimack River, shelf, and Plum Island Sound. The net water flux from Plum Island Sound to the Merrimack River varies with the interaction between tide, river discharge, and wind forcing. This interaction, in turn, affects the salt transport from this system to the shelf. Since the resulting water transport into the shelf significantly varies with the variability of the wind, models that fail to resolve this complex estuarine and shelf system could either overestimate or underestimate the salt content over the shelf.

Citation: Zhao, L., C. Chen, J. Vallino, C. Hopkinson, R. C. Beardsley, H. Lin, and J. Lerczak (2010), Wetland-estuarine-shelf interactions in the Plum Island Sound and Merrimack River in the Massachusetts coast, *J. Geophys. Res.*, *115*, C10039, doi:10.1029/2009JC006085.

1. Introduction

[2] One of the most important problems in the coastal ocean modeling is to simulate the river discharge low-salinity plume or front over the shelf. Because of the limitation of model resolution and computational resource and difficulties in resolving complex geometry and bathymetry of estuaries, the current modeling approach treats a river as a point source or as a simplify channel, with no consideration of the two-way shelf-estuarine interaction. However, most rivers terminate at the coast as a complex network of sounds, inlets, tidal creeks, and intertidal zones. The interaction between a major river and its network of sounds and inlets and its impact on the shelf plume dynamics, to the best of our knowledge, has not been well explored in estuarine and coastal modeling. For example, the Merrimack River Mouth (MR), in northeastern Massachusetts, is connected with the Plum Island Sound (PIS) to its south, a complex wetland estuary characterized with extensive salt marsh, tidal creeks, and irregularly shaped small islands (Figure 1). Since the tidal excursion in PIS is comparable with the spatial scale of the estuary and the tidal amplitude (~3 m) is of the same order of magnitude to mean water depth [*Vallino and Hopkinson*, 1998], it is clear that the MR-PIS is an integrated estuarine system, which cannot be dynamically separated if there is significant water and salt exchange between them. In addition, if there is a considerable water flux between the shelf and PIS, then an estuarine-shelf model driven by the MR discharge without inclusion of PIS could either overestimate or underestimate the spatial

[1]School for Marine Science and Technology, University of Massachusetts-Dartmouth, New Bedford, Massachusetts, USA.
[2]Marine Biological Laboratory, Woods Hole, Massachusetts, USA.
[3]Department of Marine Science, University of Georgia, Athens, Georgia, USA.
[4]Woods Hole Oceanographic Institution, Woods Hole, Massachusetts, USA.
[5]COAS Oregon State University, Corvallis, Oregon, USA.
[6]Marine Ecosystem and Environment Laboratory, College of Marine Science, Shanghai Ocean University, Shanghai, China.

0148-0227/10/2009JC006085

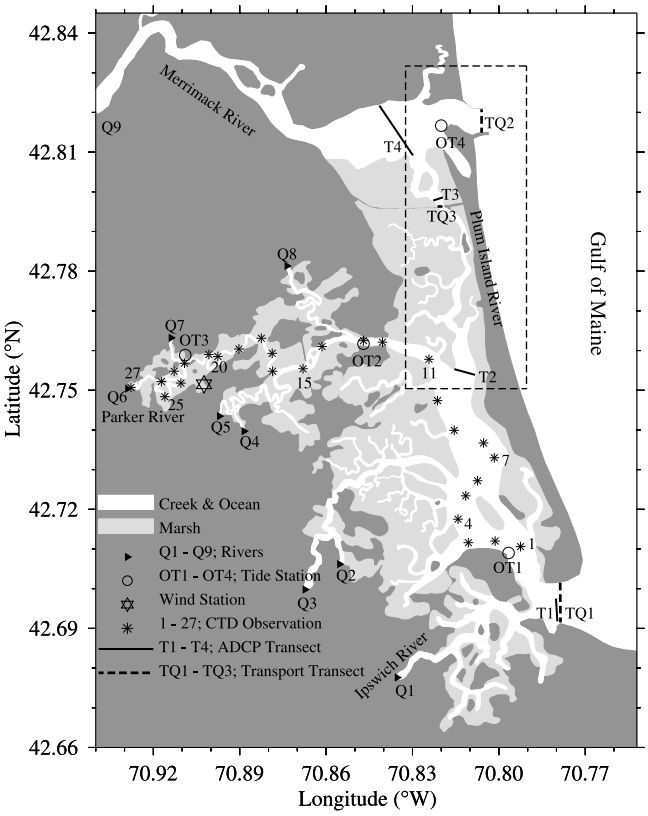

Figure 1. Bathymetry of the Plum Island Sound (PIS) and Merrimack River (MR) including station and transect locations.

distribution and temporal variability of the low-salinity plume over the shelf.

[3] As one study site of the Long-Term Ecological Research (LTER) program funded by the U. S. National Science Foundation, the Plum Island Ecosystems LTER program (PIE-LTER) launched in 1998, seeks to understanding the long-term response of watershed and estuarine ecosystems to changes in climate, land use, and sea level rise [*Vallino and Hopkinson*, 1998]. Since the physical environment, such as salinity, currents, and flooding and drying of the marsh platform, varies significantly over space and time, it is difficult to understand the key biophysical driving mechanisms that alter estuarine biogeochemistry solely with spatially limited observations [*Vallino and Hopkinson*, 1998; *Crump et al.*, 2004; *Kerry et al.*, 2004]. The salinity in the main channel of PIS, for example, can change by as much as 6 PSU within an hour. This makes it difficult to resolve the spatial salt distribution with shipboard measurements.

[4] There is a critical need to develop a hydrodynamic model that is capable of simulating the complex estuarine-shelf interaction process in the PIS-MR system. The model should have flexibility in coastal geometric fitting and be capable of resolving the flooding/drying process of the intertidal zone. This system is characterized with irregular coastlines linked to numerous islands, a barrier island, creeks and narrow water passages, and ~39 km^2 (~40%) of salt marsh with an averaged height of 1.2 m above mean sea level. The high-resolution (~5 m) topographic data obtained by LIDAR for PIE shows that marsh elevation is generally lower in the southern region of PIS but increases northward and westward, with numerous marsh ponds embedded irregularly throughout the estuary. The marsh edge along rivers and tidal creeks is very steep. In the many areas, it resembles a vertical wall of 1–2 m height. Since the average width of PIS is only 1.3 km and the water depth is 6.0–7.0 m in the southern channel area and gradually decreases to 2.0–2.5 m in the northern area, the characteristic change in water depth over the estuarine-tidal creek-salt mash complex is a dominant controlling the spatial and temporal variation of water transport in the PIS-MR system.

[5] We have used state-of-the-art finite volume, primitive equations, coastal ocean model (FVCOM) to develop a high-resolution, tidal creek resolving, hydrodynamic model simulation of the complex field of currents and salinity in the integrated PIS-MR system (hereafter referred to as PIS-MR-FVCOM). PIS-MR-FVCOM employs a high-resolution LIDAR-based bathymetry/topography digital elevation model and includes a wet/dry element analysis algorithm to model the moving surface boundary required to simulate the flooding/draining process. Nesting with in the regional Gulf of Maine FVCOM (GoM-FVCOM) (a model that has been validated for hindcast simulation from 1995 to present) allows us to resolve the estuarine-shelf interaction process over the GoM-PIS-MR system.

[6] This paper is aimed at using PIS-MR-FVCOM to examine the physical processes controlling tidal dynamics, water exchange, and thus temporal variability and spatial distribution of salinity in the PIS; the volume and salt fluxes from the PIS to the MR; and the interaction between PIS-MR system and the western shelf of GoM. The model results are validated using observational data from previous field measurement and surveys designed specially to address model predictions.

[7] The remaining sections of this paper are organized as follows. In section 2, the PIE-MR-FVCOM is introduced and developments of numerical experiments are described. In section 3, the model simulation results are presented and model-data comparisons are made. Process-oriented studies are conducted to examine the nature of the water exchange between PIS and MR and also between PIS-MR system and the western shelf of GoM. In the section 4, some critical issues related to the estuarine modeling are discussed. Conclusions are summarized in section 5.

2. PIS-MR FVCOM and Design of Numerical Experiments

[8] The PIS-MR-FVCOM is the high-resolution subdomain model nested with the regional GoM-FVCOM. FVCOM refers to the unstructured grid finite-volume coastal ocean model, which was developed originally by *Chen et al.* [2003], which has subsequently been modified and updated [*Chen et al.*, 2004, 2006a, 2006b]. The computational domain of PIS-MR-FVCOM is shown in Figure 2, which includes the detailed geometry for tidal creeks, rivers, water passages, and intertidal salt marshes and is based on LIDAR data. In the horizontal dimension, the model is discretized using a nonoverlapped triangular grid, with a resolution of ~7.0–60.0 m in tidal creeks, ~50–100 m over salt marshes, 150 m to 2.0 km in the main water

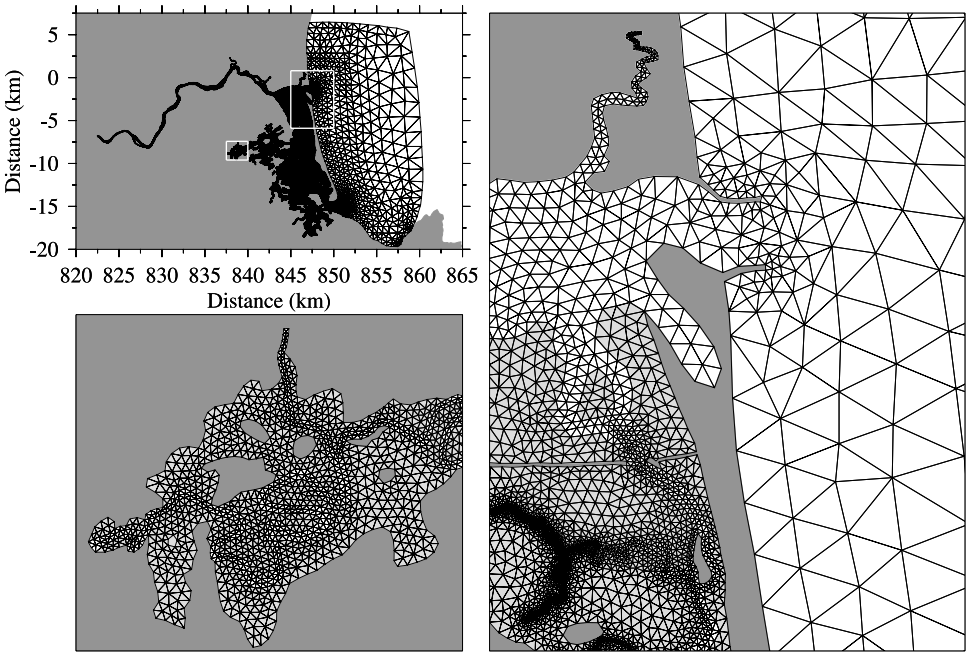

Figure 2. Unstructured triangular grid developed for the PIS-MR FVCOM computational domain. The two inserts show mesh detail for (left) the mouth of the Merrimack River and (bottom) upper Parker River.

channels of PIS and near the open boundary over the shelf of the GoM. Total number of triangular elements and nodes are 42,803 and 23,222, respectively. In the vertical dimension, seven layers are specified in the generalized terrain-followed coordinate system. Considering that the average water depth is 2–7 m in PIS, the vertical resolution is about 1.0 m or less. PIS-MR-FVCOM uses the modified Mellor and Yamada level 2.5 (MY-2.5) and Smagorinsky turbulent closure schemes for vertical and horizontal mixing, respectively [*Mellor and Yamada*, 1982; *Galperin et al.*, 1988; *Smagorinsky*, 1963], and the bottom roughness (z_0) is the uniform value of z_0 = 0.1 cm for the whole of the computational domain.

[9] To examine the physical processes controlling the temporal and spatial variability of currents and salinity in the integrated PIS-MR system, we ran the model under various forcing and initial conditions. Three types of experiments were conducted: (1) tidal simulations were obtained by driving the model using tidal elevation at the nested boundary over the shelf (hereafter referred to as Exp 1); (2) the salinity simulation involved driving the model with tidal forcing at the nested boundary but included the observed freshwater inputs and surface wind stress (hereafter referred to as Exp 2); and (3) process-oriented model runs with and without inclusion of either wind forcing or the intertidal zone to examine the contribution of the wind on the shelf-estuarine water exchange (hereafter referred to as Exp 3).

[10] For Exp 1, the model is initialized with zero velocity field and constant temperature and salinity throughout the domain. The tidal forcing consists of five major tidal constituents (three semidiurnal: M_2, N_2, and S_2; two diurnal constituents: K_1 and O_1). The values of these tidal constituents at the nested boundary are provided by GoM-FVCOM. The tidal simulation results are validated by comparison with measurement data recorded at sites OT1-OT4 (Figure 1).

[11] For Exp 2, freshwater discharge is distributed across nine rivers; namely, the Ipswich (Q1), Muddy (Q2), Egypt (Q3), Mill-1 (Q4), Mill-2 (Q5), Parker (Q6), Cart (Q7), Littles (Q8), and Merrimack (Q9) rivers (Figure 1). Runoff data for the Merrimack, Ipswich, and Parker rivers were obtained from USGS gauges. Outflows from the other six ungauged rivers were specified as a proportion of the Parker River discharge based on their watershed area relative to that of the Parker River [*Vallino and Hopkinson*, 1998], but with updated watershed area obtained from MassGIS (http://www.mass.gov/mgis/) (Table 1). Annual seepage from salt marshes into tidal creeks in PIS is estimated at $\sim 4 \times 10^8$ m^3/yr [*Gardner and Gaines*, 2008], but it is unknown what fraction of this seepage represents new groundwater addition, so we assume it to be 100%. Since tidal creeks are very narrow and tidal excursion is larger than PIS geometric scale [*Vallino and Hopkinson*, 1998], the estimated freshwater input due to groundwater was simply added to the river discharge.

[12] The initial conditions of temperature and salinity were specified using hydrographic field measurement data taken along the PIS and Parker River on 12 April 2005 and data assimilated from GoM-FVCOM for the shelf. The PIS survey began at 13:34 PM in the southern area of PIS at station 1 and ended at 15:27 PM in the Parker River at station 27 (Figure 1). The simulation started at 13:00 PM, 12 April 2005 and continued to 13 May 2005, with real-time tidal forcing, river discharge, and observed winds. The model results were validated by comparison with hydrographic survey data collected on 6 May 2005.

[13] During the simulation period, the averaged freshwater runoff is 600 m^3/s in the MR, 10 m^3/s in the IR and 2.5 m^3/s

Table 1. Relationships Used to Obtain River Discharges From the Three USGS Gauged Stations[a]

River Q	River Name	Discharge Into the System
Q1	Ipswich	1.197 $Q1_{Gauge}$
Q2	Muddy	0.08768 $Q6_{Gauge}$
Q3	Egypt	0.1553 $Q6_{Gauge}$
Q4	Mill 1	0.1022 $Q6_{Gauge}$
Q5	Mill 2	0.6032 $Q6_{Gauge}$
Q6	Parker	1.147 $Q6_{Gauge}$
Q7	Cart	0.1087 $Q6_{Gauge}$
Q8	Littles	0.3116 $Q6_{Gauge}$
Q9	Merrimack	1.0 $Q9_{Gauge}$

[a]$Q1_{Gauge}$, Ipswich; $Q6_{Gauge}$, Parker; $Q9_{Gauge}$, Merrimack Rivers. Numbers reflect the relative watershed size to the corresponding gauged watershed size.

in the PR. Wind data used to drive the model were based on meteorological measurements from the PIE-LTER weather station located near the upper Parker River (Figure 1). Wind direction varies significantly with time, with an averaged speed of 1.3 m/s. *Chen et al.* [2008] noted that in the Satilla River, due to large drag forcing, the wind stress over the salt marsh is significantly weaker than the open water body in the main channel. Following their approach, wind stress over the marsh is multiplied by a factor of 0.2. A linear interpolation is made over elements around the boundary between marsh and open water to avoid discontinuities.

[14] The MR is connected to PIS via the Plum Island River (PIR): a small river with a length of ~5.3 km, a width of ~200 m, and an averaged depth of ~2.5 m. The model results showed a significant water exchange between PIS and MR and shelf-PIS. To validate these fluxes, we surveyed currents using ADCP on transects across the mouth of PIS (T1), at the southern and northern areas of the PIR (T2 and T3) and across the MR (T4) (Figure 1) on 24 July 2008. The volume flux was estimated at these transects and compared with the model-predicted fluxes from the 2005 model run, without correcting for difference in discharge or tidal amplitudes.

[15] For Exp 3, the Exp 2 simulation was rerun by (1) removing the wind forcing, (2) treating the intertidal salt marsh as upland, and (3) fixing the river discharge at the observed largest and smallest rates. A large number of particle traces were released at selected locations in the PIS and MR at different tidal stages under these various physical conditions to illustrate the unique feature of water exchange in the integrated PIS-MR-shelf system.

3. Model Results and Comparisons With Observations

3.1. Tidal Simulation

[16] The PIS-MR-FVCOM has captured the 3-D flooding/drying processes in the integrated PIS-MR estuary. The tides flood in and drain out of this area twice a day with a dominant frequency at the M_2 tide. At high water, surface elevation during the spring tide is over 1.7 m and 98% of the marsh area is covered by water (Figure 3a), while the surface elevation during neap tide is lower than 1.0 m and only areas close to channels and PIS are flooded (Figure 3b). At low tide, water drains back to the main channels and tidal creeks. Likewise, wetted area at low tide is significantly less during spring tides than in neap tides (Figure 3c versus 3d).

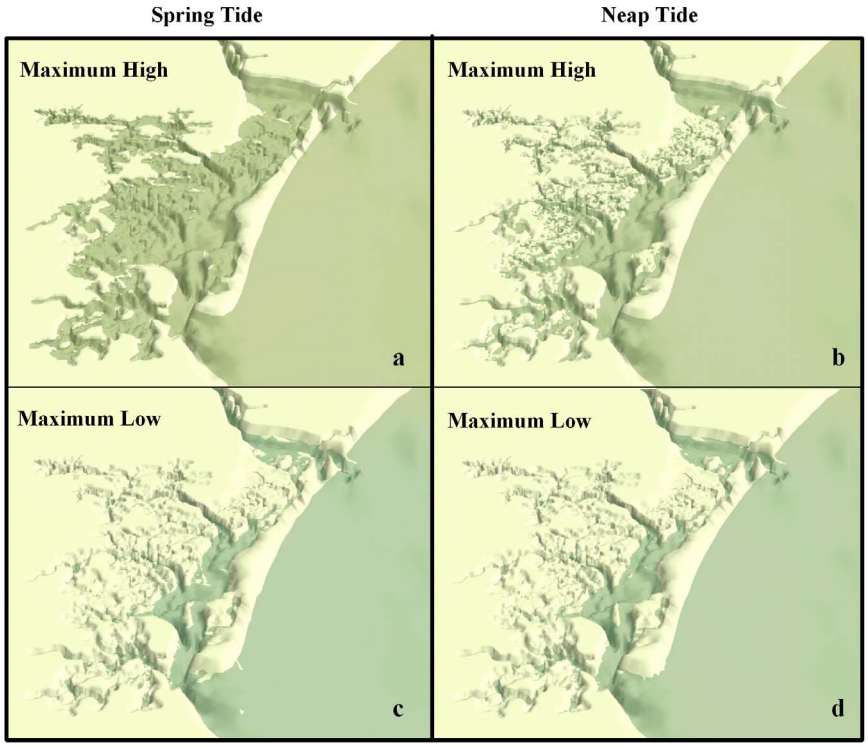

Figure 3. Projected 3-D views of the extent of flooding and drying at high and low tidal stage. (a) Spring and (b) neap maximum high tides and (c) spring and (d) neap maximum low tides.

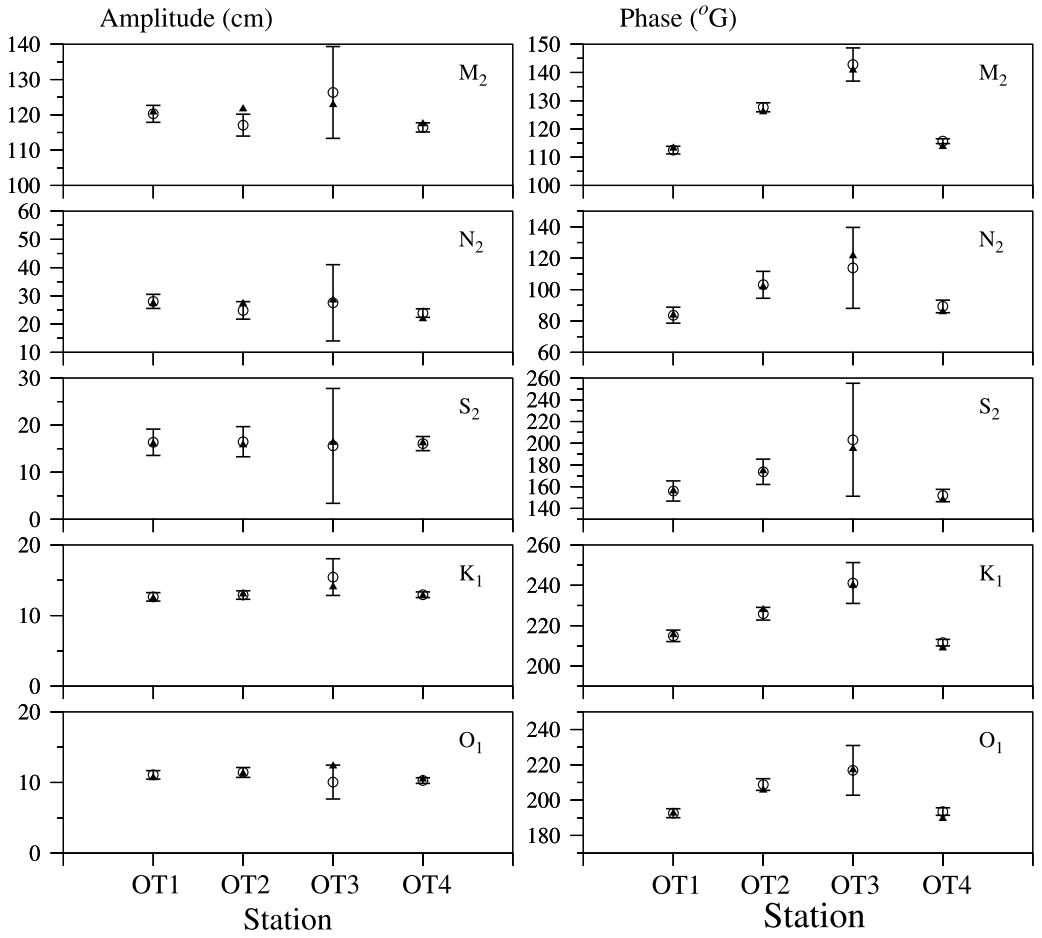

Figure 4. Comparison between model-predicted (solid triangles) and observed (open circles) (left) amplitudes (cm) and (right) phases (°G) for M_2, N_2, S_2, K_1, and O_1 tidal constituents at four tidal gauges. The location of stations OT1–OT4 are given on Figure 1.

[17] The tidal simulation results are validated by comparison of model-predicted tidal elevation with observations at tidal measurement sites OT1-OT4 (Figure 1 and Figure 4). Tidal stations OT1, OT2, and OT3 are located at the south of PIS, Massachusetts Route 1A Bridge and Middle Road Bridge, respectively, and OT4 is at the mouth of the MR. The data used for the harmonic analysis were from the entire 2002 measurement year at PIE-LTER stations OT1-OT3 and from the 26 May to 28 October 1989 measurements at OT4 (NOAA station ID: 8440452). With the 5 m resolution bathymetry from LIDAR, the model-computed amplitudes and phases of M_2, N_2, S_2, and K_1 and O_1 are in good agreement with observation (Figure 4). The standard deviation of the residuals between model and observed amplitudes and phases are 1.4 cm and 0.54°G for the M_2 tide, 0.8 cm and 2.1°G for the N_2, 0.3 cm and 1.8°G for the S_2, 0.3 cm and 1.5°G for the K_1, and 0.5 cm and 0.9°G for the O_1. Model predictions are well within the level of the measurement uncertainty (Figure 4). The observed values at OT3 exhibit a larger uncertainty because this site is located in a very shallow region and at the boundary of the estuary and salt marsh where the tidal flushing is active [*Zhao et al.*, 2006] and freshwater discharge alters tidal amplitude and harmonics.

[18] The model-computed amplitudes and phases of tidal elevation vary significantly in space. For example, the amplitude and phase of the M_2 tide are about 120 cm and 112.5°G at OT1 near the southern mouth of PIS, but change to 117 cm and 127.7°G at OT2 in the lower Parker River, and increase to 126 cm and 142.9°G at OT3 in the upper Parker River. A tidal wave entering PIS from its southern entrance takes about 31.4 min to arrive at OT2 and additional 31.4 min to arrive at OT3. Along the PIR, the amplitude and phase of the M_2 tide decrease from 118.0 cm and 122.5°G at the south to 110.0 cm and 120°G at the north (Figure 5a). The mouth of the MR is characterized by a low tidal surface elevation center (Figure 5a). This low water level center features an oscillating pattern.

[19] Correspondingly, residual currents form a clockwise flow in the mouth of the MR as well as south of the MR along the shelf, with a spatial scale comparable to local geometry and a speed of 10–50 cm/s (Figure 5b). The model predicts a net northward residual flow of ~30 cm/s in the PIR (Figure 5b), implying that PIS is a source of water flowing into the MR.

3.2. Salinity Simulation

[20] The PIS-MR-FVCOM predicts that salinity in this integrated estuarine-shelf system varies considerably in

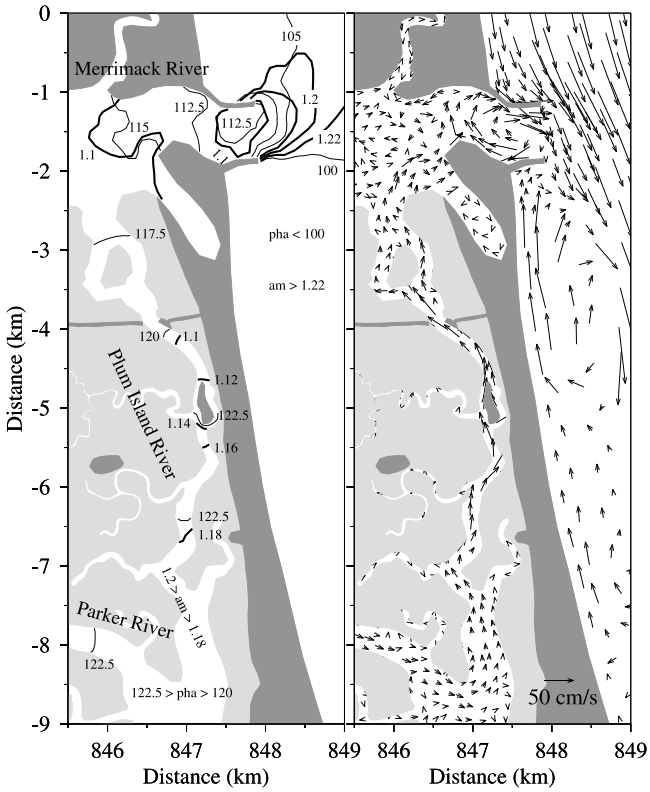

Figure 5. Co-tide chart and residual current for selected region in the PIR and mouth of MR (dash rectangular box in Figure 1). (a, left) Coamplitudes (m) and cophases (°G) of the M_2 tidal elevation in PIR region; (b, right) M_2 tide residual current.

space and time during the simulation period of April to May 2005 (Figure 6). The salinity difference at ebb and flood tides was ~5.0 PSU at the southern entrance of PIS and can reach ~16.0 PSU around the mouth of the MR. During ebb tide, low-salinity water in the MR is flushed out into the GoM to form a mushroom-like plume on the shelf. A similar process occurs in the southern entrance of PIS, although salinities are relatively high there. During flood tide, salt water is pushed into the MR, which forces low-salinity water southward into the PIR, where it mixes with surrounding water and enters PIS. The same inward saltwater intrusion also occurs in the southern entrance of PIS, which forces low-salinity water from the Sound northward and westward into surrounding subestuaries. As a result of the saltwater intrusion from the MR and PIS during the flood tide, a large salinity gradient forms between northern PIS and southern PIR (Figure 6b).

[21] The distribution of the model-predicted salinity is in good agreement with observations. Model output was compared at the same times and locations of a hydrographic survey conduced on 6 May 2005. The survey began at 9:52 AM, about 1.5 h before the high tide and completed in the upper Parker River at 11:32 AM, with 27 stations over a 21 km (Figure 1). At each station, CTD casts averaged approximately half a minute. The observations show that salinity drops from 28.3 PSU at station 1 to 0.1 PSU at the station 27, with a moderate gradient around stations 9–12 where water masses from PIS-MR and Parker River meet (Figure 7a). Multiply water sources form three salinity zones along PIE. Zone 1 is characterized by a water salinity range of 24–28 PSU, which results from the intrusion of water from the inner shelf into the southern bay of PIS. Zone 2 is defined by water in the 6–24 salinity range, which results from the mixing of water from PIS, MR, and Parker River.

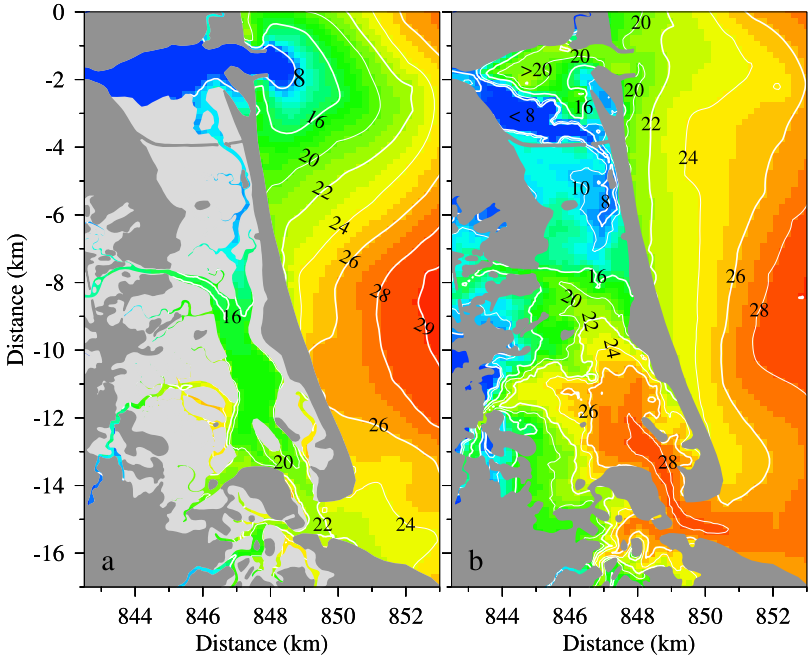

Figure 6. Modeled salinity distribution in the PIS and Merrimack River at the transition (a) of ebb to flood and (b) of flood to ebb.

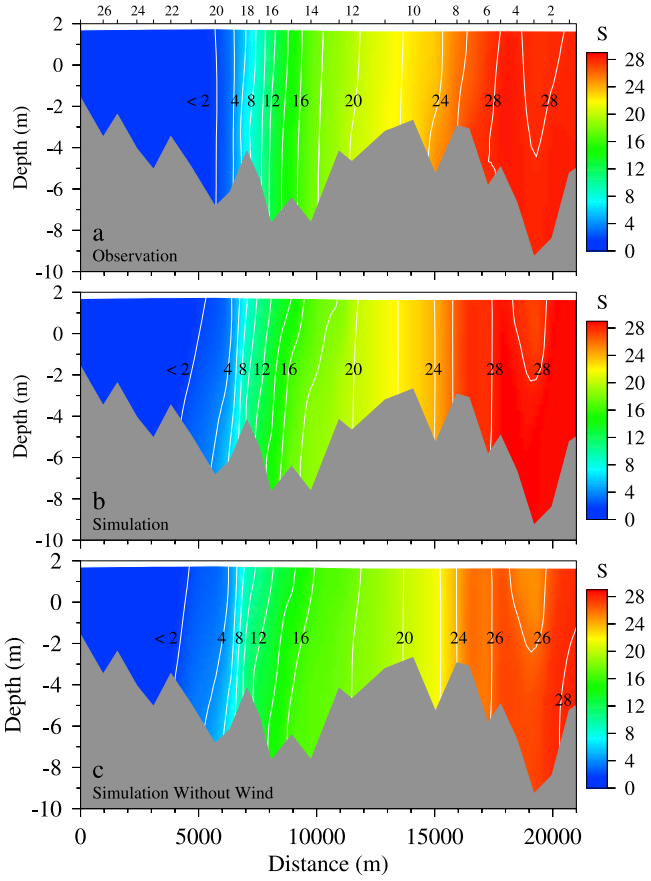

Figure 7. Comparison of (a) the vertical and horizontal salinity distributions observed and model-predicted (b) with wind forcing and (c) without wind along the ship-borne CTD transect from stations 1 to 27 on 6 May 2005. The number labels along the top of Figure 7a correspond to station numbers shown as asterisks in Figure 1.

Zone 3 occurs in the upper Parker River with a salinity range of <6 PSU, where freshwater mixes with that from PIS and MR. To account for nonsynoptic sample collection, model outputs were generated every minute over the CTD survey and only those outputs that corresponded in time and location to the CTD casts were chosen for comparison to observations. As a result, the timing difference between model output and field measurements are not larger than 15 s. For observed wind and tidal forcing, the simulation results match well with the observations, not only qualitatively in along-river distribution but also quantitatively in the salt content at each measurement station (Figure 7b). The impact of wind on salinity mainly occurs in zone-1, an area close to the southern entrance of PIS from the inner shelf. In the simulation without wind, salinity in zone 1 is ~2.0 PSU lower and stratified, suggesting that wind plays an essential role in eliminating stratification in the southern mouth of PIS and transporting high salinity GoM water during the study period.

[22] It should be pointed out that the three-zone salinity structure exists over all time. Data in Figure 7 occurs around maximum high tide. During the ebb tide, the salinity distribution shifts southward, during which water in zone 2 may reach the inner coastal shelf to form the lower salinity plume (Figure 6a), a portion of which moves back into PIS during flood tide (Figure 6b). The excursion scale of the water movement in these zones is similar to the tidal excursion scale, with a variation over the seasons associated with changes in river discharge, coastal shelf salinity, and current conditions and strength of tidal flushing (i.e., neap versus spring tide) as well.

3.3. Water Exchange

[23] To examine the water exchange between PIS and MR, we estimate the water and salt fluxes at TQ1 (transect across the mouth of PIS), TQ2 (transect across the mouth of the MR), and TQ3 (transect across the PIR, the water passage linking PIS and the MR) (Figure 1). The flux value at each transect is calculated by averaging the flux over a tidal period between two successive high tides for both spring and neap tides (Table 2). Because of tidal phase differences at TQ1, TQ2, and TQ3, we do not expect the sum of these fluxes to equal zero, because phase differences affect the timing of maximum currents, which can lead to internal water storage in the estuary (Figure 8).

[24] Transport time series (Figure 8a) also provide a direct view of the net flux across TQ1 and TQ2. For TQ1, the largest flux during a tidal cycle occurs during flood tide, so that tidally averaged flux is positive (inflow from the shelf to PIS). For TQ2, the largest flux occurs during ebb tide, so that tidally averaged flux is negative (outflow from the MR to the shelf). These transport features do not change from neap and spring tides (Figures 9b and 9c). For spring tide, for example, the model predicts a net outflow at the mouth of MR (TQ2) at a transport value of ~−907 m^3/s (Table 2). This outflow accounts for a freshwater discharge of ~840 m^3/s, and a net flux of ~77.7 m^3/s through TQ3 from PIS to the MR. This suggests that in addition to freshwater discharge from the MR, a net flux from PIS accounts for ~8.6% of the total MR outflow onto the shelf. Since the PIS water is significantly more saline than the MR water, the net transport from PIS to the MR can significantly modify the salinity of the MR outflow. The net transport from PIS to the MR comes from two major sources: one is from a net inflow of ~54.5 m^3/s at the southern mouth of PIS and the other is the sum of freshwater river discharges of ~59 m^3/s into PIS. Although not all of these waters flow into the MR, it is clear that PIS has a net flux into the MR. This finding is also true for neap tide and also for the case with removal of wind forcing (Table 2), suggesting that the MR, PIS and shelf are an integrated estuarine-shelf system and a model for the MR without inclusion of PIS could cause the underestimation of the water transport and thus an inaccurate salt transport from the MR to the shelf.

[25] To validate our model results regarding transport between PIS and the MR, we conducted ship-board surveys to measure the currents in the PIS-MR region on 24 July 2008. Four transects are examined here, T1, T2, T3, and T4 (Figure 1), where ADCP measurements (RDI Rio Grande) were performed at 11:55, 18:01, 17:24, and 14:15, respectively. Transport fluxes were estimated using WinRiver II (RD Instruments) and were compared to model-predicted fluxes at the similar tidal phase in the April–May 2005 PIS-MR FVCOM simulation. Although the observed and model-predicted fluxes were for slightly different tidal phases and significantly different river discharges, model

Table 2. Net Flux of the Water Transport (m^3/s) Cross the Mouth of PIS (TQ1), Mouth of MR (TQ2), North of PIR (TQ3), and River Discharge in PIS and MR for the Exp 2 and Exp 3 Simulations[a]

	With Wind		Without Wind	
	Neap Tide	Spring Tide	Neap Tide	Spring Tide
TQ1	54.9	54.5	25	97.4
TQ2	−404	−907	−425	−944.8
TQ3	73	77.7	100	126
PIS Rivers	33	59	33	59
MR River	340	840	340	840
TQ1-TQ3 + PIS Rivers	14.9	35.8	−42	30.4
TQ2 + TQ3 + MR River	9	10.7	15	21.2

[a]TQ1 > 0 flux into PIS, TQ2 > 0 flux into MR, TQ3 > 0 northward flux into MR.

predictions are within ±12.5% of observed values (Table 3). The difference between model-predicted and observed values is mainly due to the coverage limit of the measurement in the shallow area in addition to seasonal variation in winds, freshwater discharge and stratification. For example, T1 did not cross the entire mouth of PIS because the northern part of the region was too shallow for the boat to enter. The water transport in these areas was estimated by the linear extrapolation from the interior where the ADCP measurement data were available. A 12.5% difference found between the observation and model is within an uncertainty of the current variation cross this transect. Similar situations also applied for T2, T3, and T4. The measurements support our model results that a significant net water flux from PIS to the MR occurs, so that the PIE needs to be studied as an integrated river-estuarine-shelf system with the inclusion of the MR and shelf.

3.4. Particles Trajectories

[26] The net flux through PIR from PIS to the MR raises a fundamental dynamics question on whether or not there is a recirculation from the MR, to the shelf and back into PIS. To examine this question, we conducted a Lagrangian neutral-buoyant particle-tracking experiment under the flow field predicted by PIS-MR FVCOM for the April to May 2005 simulation. To identify the impact of wind forcing, we repeated this experiment with removal of wind forcing in the model.

[27] In the case with winds, the particles released at the maximum flood tide in the MR during both spring and neap tidal cycles followed a main trajectory flowing onto the

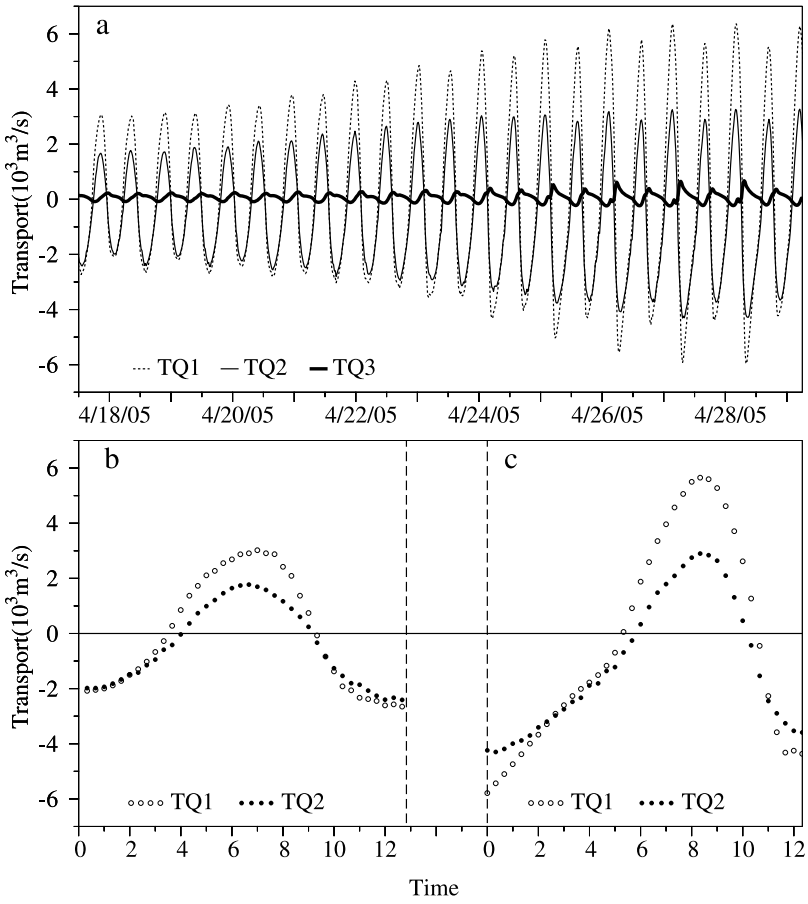

Figure 8. Water fluxes predicted across transects TQ1, TQ2, and TQ3 by PIS-MR FVCOM. (a) Time series of the simulated water flux through transects TQ1 (solid line), TQ2 (dashed line), and TQ3 (heavy solid line) from neap to spring tide in April 2005. (b) Simulated water flux during a neap tide cycle across transects TQ1 and TQ2. (c) Simulated water flux during a spring tide cycle across transects TQ1 and TQ2.

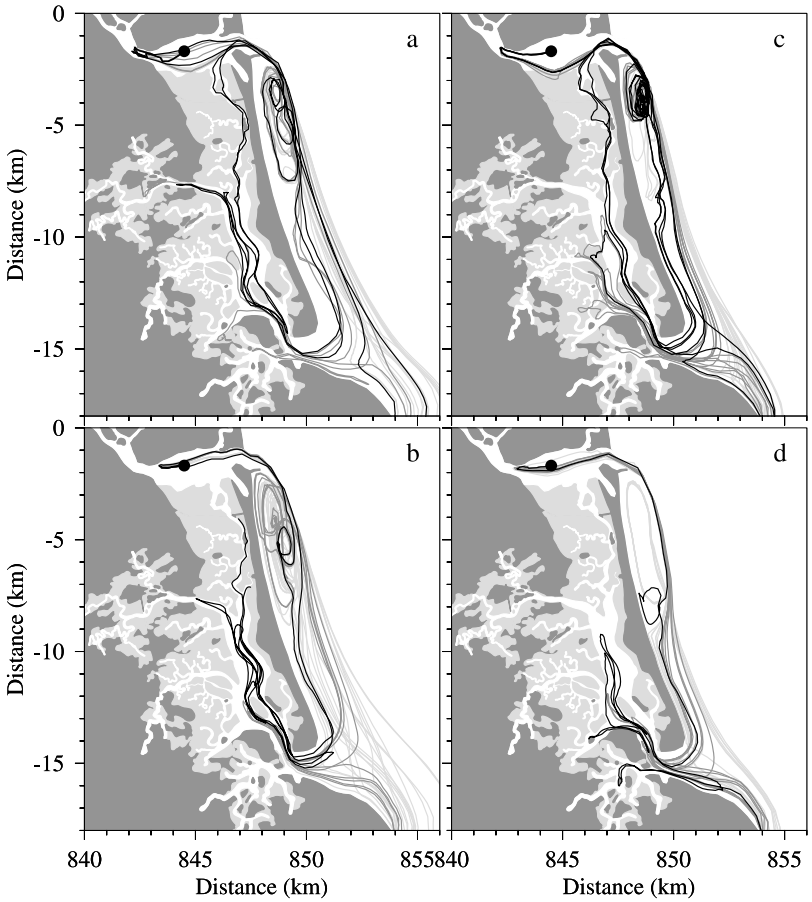

Figure 9. Trajectories of particles released in the Merrimack River. (a) Particles released at maximum spring flood tide. (b) Particles released at maximum neap flood tide. (c) Same as Figure 9a, but without wind forcing. (d) Same as Figure 9b, but without wind forcing.

shelf and then turned clockwise to flow southward along the shelf (Figures 9a and 9b). For the spring tide case, among the 50 particles released, 7 entered PIS via the southern mouth, and 2 recirculated back into the MR through the PIR, with a total circulation time scale of 7–9 days (Figure 9a). For the neap tide study, 11 particles entered PIS, of which two recirculated back toward the MR but became embedded on the PIR marshes (Figure 9b). The behavior of particles released at maximum flood tide in PIS (Figures 10a and 10b) depends on tidal amplitudes and induced currents. For the spring tide case, all 50 particles moved into the MR, where 37 of them continued onto the shelf, with 6 these recirculated back into the MR through PIS (Figure 10a). For the neap tidal case, all particles eventually became embedded on the marshes of PIR, although several particles tended to move out of PIS during the first few tidal cycles (Figure 10b). Particles released in the mid Parker River at ebb tide flowed out to the mouth of PIS at first but then were advected back into PIS. Once reaching the northern end of PIS, some continued further and entered the MR through the PIR (Figure 11a). Similarly, particles released at the end of ebb tide in the northern PIR near the MR can be advected to PIS via the PIR (Figure 11b). A portion of these particles moved back and forth through PIR between the MR and PIS over several tidal cycles, while others flowed from the MR into PIS via the shelf.

[28] The influence of wind on particle movement was significant over the shelf and near the mouth of the MR and the southern entrance of PIS, but not inside the river and sound. For the case without wind forcing, the majority of particles released at maximum flood tide recirculated between the MR and PIS via the PIR for the spring tide study (Figure 9c). Although the tidal currents were much weaker during the neap tide period, the majority of particles still showed a recirculation tendency as shown during spring tide (Figure 9d). A similar tendency was also evident for particles released in PIS during the flood tide period for both spring and neap tides (Figures 10c and 10d); however, particles were able to complete the full circulation pattern (PIS-PIR-MR-shelf-PIS) during neap tide when wind forcing was not included (Figure 10d).

Table 3. Comparison of Model-Predicted and Observed Fluxes (m^3/s) at Transects T1–T4 in Figure 1

	Observation	Model
T1	1309	1496
T2	−251	−260
T3	100	111
T4	1750	1774

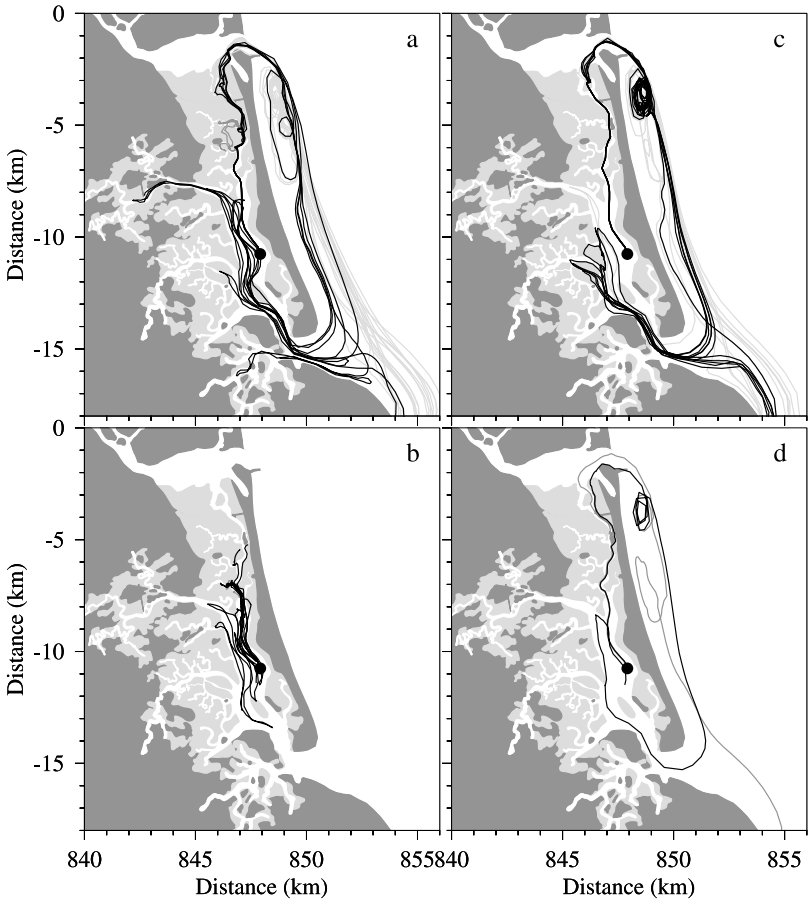

Figure 10. Trajectories of particles released in Plum Island Sound. (a) Particles released at maximum spring flood tide. (b) Particles released at maximum neap flood tide. (c) Same as Figure 10a, but without wind forcing. (d) Same as Figure 10b, but without wind forcing.

[29] The Lagrangian particle-tracking experiment results suggest that there is an anticyclonic residual circulation in the PIS-MR-shelf integrated system. This recirculation tends to be intensified when either the wind is relaxed or downwelling-favorable wind over the shelf and is weakened by upwelling-favorable winds. A regional ocean model that treats the MR as an inland point source without inclusion of the surrounding PIS and intertidal zone could overestimate

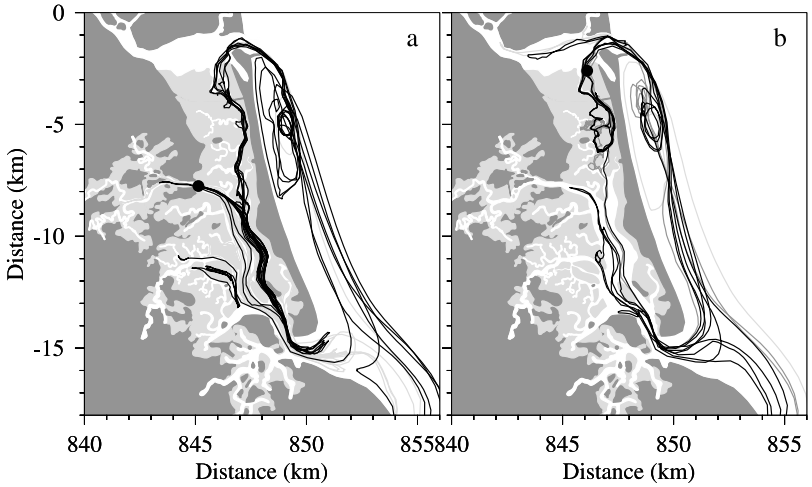

Figure 11. Trajectories of particles released in (a) the mid Parker River at maximum ebb tide and (b) at the northern mouth of Plum Island River at the end of ebb tide.

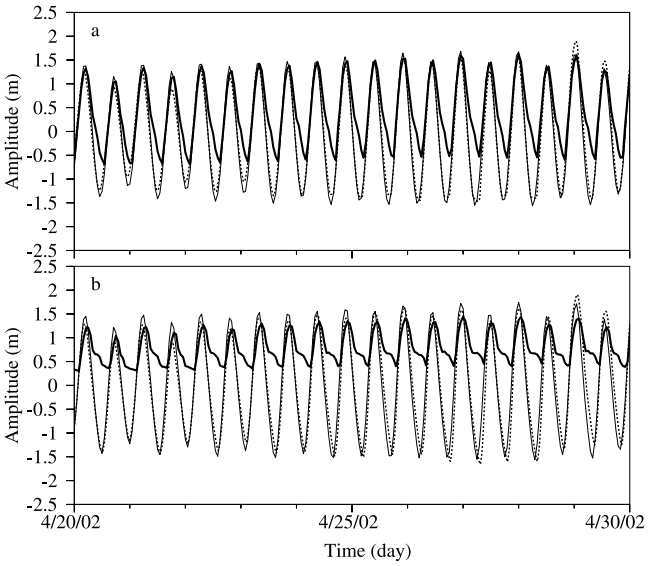

Figure 12. Comparison of model-predicted and observed water levels at (a) southern PIS (OT1 in Figure 1) and (b) Middle Road Bridge (OT3 in Figure 1) during 20–30 April 2002. Dashed line, observed water levels; solid line, model-predicted water levels with marsh topography obtained by LIDAR; heavy solid line, model-predicted water level with marsh topography fixed uniformly at 1.0 m NAVD88.

the along-shelf buoyancy flow into the downstream Mass Bay region, because a portion of the outflow water might recirculate back into the estuarine system through PIS.

4. Discussion

[30] The unstructured grid PIS-MR FVCOM is able to resolve the integrated estuarine-intertidal wetland-shelf system that has not been well explored in previous studies of this coastal region. The complexity of the dynamic processes detected in this study calls attention to the need of future estuarine modeling since it is standard practice to simplify shelf models by only considering river inputs without inclusion of the estuarine network connected to the river. Also, model results obtained in previous model studies of the MR need to be examined with caution if they lack interaction of the MR and PIS and intertidal wetland.

[31] FVCOM is well suited to explore the complex multiscale interactions between estuaries and shelf. The success of this model, however, depends on the accuracy of bathymetry used in the model. In the PIS-MR FVCOM experiments, we found that the elevation of the marsh is critical for accurate tidal simulation. At the beginning of our experiment, due to the lack of topographic data over marshes, we simply treated PIS as a coastal-plain estuary by assigning the marsh elevation a constant value of 1.0 m above the local mean sea level. Under this assumption, the model-predicted tidal wave propagation into PIS was unrealistic, in that it failed to accurately resolve tidal currents during ebb tides. The distortion of the tidal wave increased with distance from the open boundary. Examples are given here for stations OT1 and OT3, which show that the model-predicted water level amplitude of water elevation at OT1 (southern PIS) is about 50% lower than that observed during ebb tide (Figure 12a) and water level never drops below mean sea level at OT3 (upper Parker River at Middle Road Bridge) (Figure 12b). This feature did not change even with increased the tidal amplitude impulse at the open boundary. The availability of high-resolution LIDAR (Light Detection and Ranging) data appears critical for accurately modeling estuarine circulation. Made possible by remote sensing technology [*Guenther*, 2007], LIDAR data for PIS includes more than 4 million points with an average resolution of ~5 m. Using this high-resolution topographic data combined with GPS-based bathymetry surveys to configure the PIS-MR-FVCOM, the model was capable of producing an accurate spatiotemporal simulation of tidal elevation in PIS-MR without need for tuning the open boundary forcing (Figures 4 and 12). Our results suggest that attention should be paid to improving the local topography/bathymetry for any estuarine modeling. Tuning model parameters to match the tidal observation under inaccurate bathymetric conditions may provide the right answer but for the wrong physics.

[32] The observations in the PIS have shown a large variability in salinity in time and space as a result of large tidal excursion scale, variability in freshwater discharge, and estuarine-salt marsh interaction. This is a common feature in tidally dominant estuaries [*Chen et al.*, 2008]. For this reason, ship-board observations were hard to compare to modeled spatial distributions of salinity in the PIS Estuary because slight errors in space or time can produce large changes in salinity. Model-data comparison needs to be made at the exact same time and location where measurements are conducted. Figure 13 shows the model-data comparison of the salinity in May 2005. Station numbers 1, 11, and 20 are the three measurement sites selected from the CTD survey track from the south (near the mouth of PIS) to the lower Parker River. In addition to good agreement found between computed and observed salinities, the model shows that salinity varied over a range of 19.6–29.3 PSU at station 1, 14.1 to 22.8 PSU at station 11, and 1.2 to 3.4 PSU at station 20. Since model output occurs at the same interval as the model time step, slight differences in the model and observation times can cause a noticeable disagreement between the model and observation.

[33] The PIS-MR-FVCOM is the first hydrodynamic model of the PIE that includes the MR. The model suggests that the PIR transports relatively high salinity PIS water into the MR but also allows low-salinity MR water to enter PIS during flood tide. The fresh MR water decreases the salinity over the PIR marshes (Figure 6b), which may be contributing to the Phragmites invasion in that area [*Buchsbaum et al.*, 2006]. Our experiment reveals that the nonlinear interaction of tidal currents over the estuarine-wetland may produce a low-frequency (~3 days) oscillation in tidal currents. Because of this, the flux at the mouth of the MR will not balanced the flux at the southern mouth of PIS with inclusion of river inflow if the flux is estimated over either a tidal cycle or after removal of tidal signals using harmonic analysis. To insure mass conservation in the model, we have conducted a series of numerical experiments to estimate the transport under various forcing and bathymetric conditions. The simplest case involved driving the model by only M_2

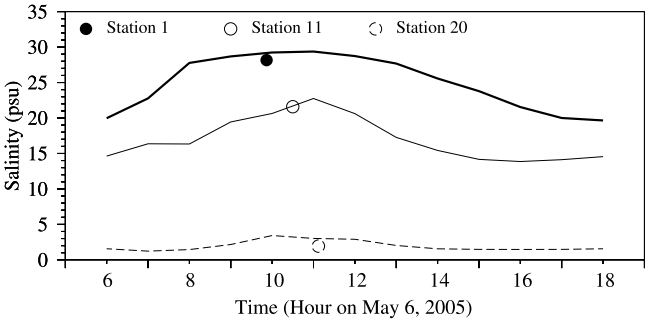

Figure 13. Comparison of model-predicted (lines) and observed salinity at CTD stations 1, 11, and 20 (see Figure 1).

tides for the computational domain without inclusion of the intertidal wetland. For a high constant freshwater discharge case with rates of 1350 m^3/s into the MR and 97 m^3/s into PIS, the tidally averaged outflow fluxes through the mouths of the MR and PIS are 1364.8 and 82.2 m^3/s, which precisely balance total freshwater input. In this case, the model predicts a net flux of 14.8 m^3/s through the PIR from PIS to the MR. For a low freshwater discharge case of 42.25 m^3/s into the MR and 0.126 m^3/s into PIS, the tidally averaged flux of the MR-PIS system is also balanced, with a net inflow of 127.09 m^3/s through the southern mouth of PIS and a net outflow of 169.67 m^3/s through the mouth of the MR. In this case, the model predicts a net flux of 127.22 m^3/s from PIS to the MR. Both experiments clearly demonstrate that the finite-volume algorithm used in the PIS-MR-FVCOM ensures the volume and mass conservation in the computational domain.

[34] Repeating these two test studies with inclusion of the intertidal wetland, we found that the flux from PIS to the MR increased to 32.41 m^3/s for the high freshwater discharge case and 139.28 m^3/s for the low river case. It is clear that the net flux from PIS to the MR varies with the strength of the freshwater discharges and wind conditions. One of the remaining questions for this study is whether or not the 3 day oscillations found in the model with inclusion of the marsh flooding or drying processes over the intertidal wetland is accurate. Since the volume flux is averaged over a period exceeding 3 days, this suggests that the 3 day oscillation is not a result of numerical errors caused by the wetting/drying numerical techniques used to account for the moving boundary. Because the surface elevation is proportional to the divergence or convergence of the integrated volume flux, we expect this low-frequency signal from the spectral analysis of surface elevation records should be observable. Unfortunately, all the surface elevation data recorded in PIS have a gap almost every 14 days, so we could not use existing data to validate our modeling finding. We believe that this low-frequency oscillation should appear in other estuaries with intensive intertidal salt marshes. This question needs to be addressed in future current or surface elevation measurements.

5. Conclusions

[35] The PIS-MR FVCOM is developed as one component of the multiscale modeling framework of the Northeast Coastal Ocean Forecast System (NECOFS). This model was used to examine the wetland-estuarine-shelf interaction processes in PIS and the MR system in the Massachusetts coast that is part of the PIE-LTER program. The model has successfully simulated the 3-D marsh and tidal flat flooding/drying process, temporal variability and spatial distribution of salinity as well as the water exchange flux through the water passage linking PIS and the MR. Both the flux estimation and Lagrangian trajectories suggest that there is a complex recirculation loop around the MR, shelf, and PIS. The net flux from PIS to the MR varies with the magnitude of freshwater discharge into the MR and PIS and the strength of wind forcing. The northward PIR flux is larger when winds vanish or are weak and when freshwater discharge conditions are low. The existence of this net flux is a result of nonlinear tidal rectification. In order to accurately obtain alongshore salt transport toward Mass Bay and to accurately simulate the salt balance in the MR, both regional and estuarine models need to include the detailed geometry of the MR and PIS together with the shelf.

[36] **Acknowledgments.** The development of FVCOM is supported by NSF grants (OCE-0234545, OCE-0227679, OCE-0606928, OCE-0712903, OCE-0726851, OCE-0814505, ARC0712903, ARC0732084, and ARC0804029), MIT Sea Grant funds (2006-RC-103 and 2010-R/RC-116) and NOAA NERACOOS Program for the UMASS team. C. Chen's contribution is also supported by Shanghai Ocean University International Cooperation Program (No. A-2302-10-0003), the Program of Science and Technology Commission of Shanghai Municipality (No. 09320503700), the Leading Academic Discipline Project of Shanghai Municipal Education Commission (Project numbers: J50702), and Zhi jiang Scholar and 111 project funds of the State Key Laboratory for Estuarine and Coastal Research, East China Normal University (ECNU). The numerical experiments were conducted using the High Performance Computer Cluster of the Marine Ecosystem Dynamics Modeling Laboratory at the School of Marine Science and Technology, University of Massachusetts–Dartmouth, purchased through Massachusetts Marine Fisheries Institute NOAA grants DOC/NOAA/NA04NMF4720332 and DOC/NOAA/NA05NMF4721131.

References

Buchsbaum, R. N., J. Catena, E. Hutchins, and M. J. James-Pirri (2006), Changes in salt marsh vegetation, *Phragmites australis*, and nekton in response to increased tidal flushing in a New England salt marsh, *Wetlands*, *26*, 544–557.

Chen, C., H. Liu, and R. Beardsley (2003), An unstructured grid, finite-volume, three-dimensional, primitive equations ocean model: Application to coastal ocean and estuaries, *J. Atmos. Ocean Tech.*, *20*(1), 159–186.

Chen, C., G. Cowles, and R. C. Beardsley (2004), An unstructured grid, finite-volume coastal ocean model: FVCOM user manual, 1st ed., *Tech. Rep. 04-0601*, 183 pp., SMAST/UMASSD, New Bedford, MA.

Chen, C., R. C. Beardsley, and G. Cowles (2006a), An unstructured grid, finite-volume coastal ocean model (FVCOM) system, *Oceanography*, *19*, 78–89.

Chen, C., G. Cowles, and R. C. Beardsley (2006b), An unstructured grid, finite-volume coastal ocean model: FVCOM user manual, 2nd ed., *Tech. Rep. 06-0602*, 315 pp., SMAST/UMASSD, New Bedford, MA.

Chen, C., J. Qi, C. Li, R. C. Beardsley, H. Lin, R. Walker, and K. Gates (2008), Complexity of the flooding/drying process in an estuarine tidal-creek salt-marsh system: An application of FVCOM, *J. Geophys. Res.*, *113*, C07052, doi:10.1029/2007JC004328.

Crump, B. C., C. S. Hopkinson, M. L. Sogin, and J. E. Hobbie (2004), Microbial biogeography along an estuarine salinity gradient: Combined influences of bacterial growth and residence time, *Appl. Environ. Microbiol.*, *70*, 1494–1505.

Galperin, B., L. H. Kantha, S. Hassid, and A. Rosati (1988), A quasi-equilibrium turbulent energy model for geophysical flows, *J. Atmos. Sci.*, *45*, 55–62.

Gardner, L. R., and E. F. Gaines (2008), A method for estimating pore water drainage from marsh soils using rainfall and well records, *Estuar. Coast. Shelf Sci.*, *79*, 51–58, doi:10.1016/j.ecss.2008.03.014.

Guenther, G. C. (2007), Airborne lidar bathymetry, in *Digital Elevation Model Technologies and Applications: The DEM Users Manual*, Chapter 8, 2nd ed., edited by D. Maune, pp. 253–320, Am. Soc. for Photogramm. Remote Sens., Bethesda, MD.

Kerry, J., D. Boorse, and R. Buchsbaum (2004), The effect of nutrient enrichment and salinity on salt marsh invertebrates in the Plum Island Estuary, *Biol. Bull.*, *207*, 174.

Mellor, G. L., and T. Yamada (1982), Development of a turbulence closure model for geophysical fluid problem, *Rev. Geophys.*, *20*(4), 851–875, doi:10.1029/RG020i004p00851.

Smagorinsky, J. (1963), General circulation experiments with the primitive equations: I. The basic experiment, *Mon. Weather Rev.*, *91*, 99–164.

Vallino, J. J., and C. S. Hopkinson Jr. (1998), Estimation of dispersion and characteristic mixing times in Plum Island Sound Estuary, *Estuar. Coast. Shelf Sci.*, *46*(3), 333–350.

Zhao, L., C. Chen, and G. Cowles (2006), Tidal flushing and eddy formation in Mount Hope Bay and Narragansett Bay: An application of FVCOM, *J. Geophys. Res.*, *111*, C10015, doi:10.1029/2005JC003135.

R. C. Beardsley, Woods Hole Oceanographic Institution, Woods Hole, MA 02543, USA.

C. Chen, H. Lin, and L. Zhao, School for Marine Science and Technology, University of Massachusetts-Dartmouth, 706 South Rodney French Blvd., New Bedford, MA 02744, USA. (lzhao@Umassd.edu)

C. Hopkinson, Department of Marine Science, University of Georgia, Athens, GA 30602, USA.

J. Lerczak, COAS Oregon State University, Corvallis, OR 97331, USA.

J. Vallino, Marine Biological Laboratory, 7 MBL Street, Woods Hole, MA 02543, USA.